Drift wave turbulence studies on the effect of limiter/divertor plates positioning

T. T. Ribeiro[1,2], B. Scott[2], F. Serra[1]

[1] *Centro de Fusão Nuclear – EURATOM/IST Association, Lisbon, Portugal*

[2] *Max-Planck-Institut für Plasmaphysik, EURATOM Association, Garching, Germany*

Introduction: The boundary region of a tokamak plasma is best defined by the values of three quantities: $\hat{\mu} = \hat{\varepsilon}(m_e/M_i) = (c_s/L_\perp)^2/(V_e/qR)^2$, $\hat{\beta} = \hat{\varepsilon}(4\pi p_e/B^2) = (c_s/L_\perp)^2/(v_A/qR)^2$ and $C = 0.51\hat{\mu}\nu_e/(c_s/L_\perp)$, which rule the electron parallel dynamics through the inertia, the induction and the resistivity, respectively [1], where ν_e is the electron-electron collision frequency, $c_s = \sqrt{(T_e/M_i)}$ is the sound speed and q is the magnetic field pitch. The ratio $\hat{\varepsilon} = (qR/L_\perp)^2 = (c_s/L_\perp)^2/(c_s/qR)^2$, which appears folded into the previous expressions, controls the sound wave dynamics (ions) and provides a measure of the spatial anisotropy between the directions parallel and perpendicular to the background magnetic field B. In a magnetised plasma this ratio is a large number (flute mode character). In the edge of a tokamak plasma, due to the steepness of the background profiles (smallness of the profile scale length $L_\perp$), it is large enough such that, necessarily, $\hat{\mu} > 1$. This means that, the electron inertia is sufficient for the electron thermal velocity (along B) not to be considered arbitrarily fast when compared to the turbulence (plane $\perp$ to B) dynamical frequencies, resulting in non-adiabatic electrons. By the same token, $\hat{\beta} > 1$ means that the parallel (shear) Alfvén dynamics is not arbitrarily fast compared to the turbulence, so that electromagnetic effects become relevant. Finally, one also has the collisionality $C > 1$, such that, all together, the edge is in the electromagnetic collisional drift wave turbulence regime, characterised by interactions between wavelike and fluidlike motions, on space scales from $L_\perp$ down to ρ_s. The parallel spatial scales are $k_\parallel qR \sim 1$ due to higher dissipation on smaller scales [2] and larger scales are disallowed by the field line connection property of the flux geometry in a sheared B [3]. For the scrape-off layer (SOL) region, where the field lines intersect material plates, convective cell modes ($k_\parallel = 0$ for $k_\perp \neq 0$) are in turn allowed [4].

Another important aspect of the edge region is the interaction between the $E \times B$ zonal flows driven by the turbulence and the background MHD equilibrium itself (Pfirsch-Schlűter currents). This happens because the larger spatial scales in the edge turbulence are comparable to $L_\perp$ due to the relatively large value of $\rho_s/L_\perp \gtrsim 10^{-2}$. Hence, since the equilibrium background is no longer in balance due to the finite total divergence of the dynamical zonal flows, although it time averages to zero, this effect should be taken into account in a field aligned coordinate system, by adjusting the alignment of the coordinates to the temporal variation of the equilib-

rium [5]. Finally, the observed $T_i \sim T_e$, together with the fact that the vorticity acts most strongly near ρ_s [6] implies accounting for finite ion Larmor radius effects.

Model: We use the 6-moment gyrofluid model GEM [7], which includes all the above mentioned ingredients, to investigate electromagnetic turbulence and the associated transport phenomena both in the edge and in the scrape-off layer (SOL). To include the SOL region in the computations, the radial domain of the computation is extended (doubled), and in the extra half, rather than the globally consistent periodicity conditions [3] used in the inner half (edge), a standard Debye sheath form is used where the field lines strike material surfaces [4]. The effect of different poloidal positions of the material plates is studied by changing the place, along the field lines, where the Debye sheath boundary conditions are applied. In particular, a case with single limiter placed at the bottom of the plasma, and a case with two limiters, placed at the top and bottom, to isolate the region where the curvature is favourable (inboard) from the one where it is unfavourable (outboard), are addressed and compared with the case with no limiters. The model used herein is the global one, where the parameter set is local (constant), but the zonal profiles of the dependent variables are evolved in time. The initial state is a density disturbances field for both species plus an initial profile for the densities and temperatures. Profiles are later maintained by feedback dissipation towards the initial nominal values with source/sink zones at each radial boundary. The local parameter set used in the simulations is typical for the edge plasma $\hat{\beta} = 1.5$, $\hat{\mu} = 5.0$, $C = 2.7$, $\hat{\varepsilon} = 18350$, $\hat{s} = 1.0$ (magnetic shear), $\tau_i = T_i/T_e = 1$, $L_\perp = L_T = L_n/2$ and $\omega_B = 2L_\perp/R = 0.046$. These correspond to the physical quantities $T_i = T_e = 80$eV, $n_i = n_e = 2.2 \times 10^{13}$cm^{-3}, $B = 2.2$T, $R = 165$cm, $a = 50$cm, $L_\perp = 3.8$cm, $M_i = 3670m_e$ and $q = 3.1$. The grid count used is $64 \times 128 \times 16$ in radial, toroidal and poloidal directions, respectively, for the cases with adjacent edge and SOL regions.

Results: Except when explicitly mentioned, the diagnostics shown are averaged over the interval $2000 < t/(c_s/L_\perp) < 4000$, for which the system was already well into the saturated turbulent state. The transport is observed to increase when one moves from a edge only situation ($Q_e \sim 12$, in gyro-Bohm normalised units), to an edge plus SOL with the double limiter (DL) ($Q_e \sim 20$).
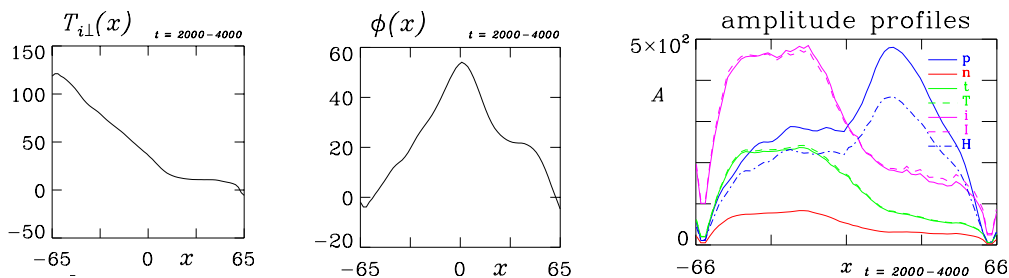

Figure 1: Time averaged zonal profiles of (a) ion temperature and (b) electrostatic potential. (c) profile of the amplitudes in the nonaxisymmetric fluctuations of $\tilde{\phi}$ ('p'), $\tilde{n}_e$ ('n'), $\tilde{T}_e$ ('t' and 'T'), $\tilde{T}_i$ ('i' and 'I') and $\tilde{h}_e = \tilde{n}_e - \tilde{\phi}$ ('H'). All for the DL case. The LCFS is at $x = 0$.

For the single limiter at the bottom (SL) of the flux surfaces, no significative change in the transport level was observed. The zonal (flux surface averaged) profile for the ion temperature is shown (Fig. 1a). The SOL region is flatter due to the higher transport level observed there, a consequence of the interchange type dynamics typical of the SOL [4]. Although not visible from this picture, in the SOL, the axisymmetric part of $T_{i\perp}$ is different on the inboard and outboard sides. The zonal part of the electrostatic (Fig. 1b) potential shows a shear layer [8, 9], which is a feature that arises naturally in this kind of simulation including both the edge and the SOL [5]. It follows from the fact that, in the SOL, the Debye sheath dissipation couples effectively the electrostatic potential to the electron temperature larger scales [4], whereas in the edge, the electrostatic potential is conditioned by the ion dissipation channels in the axisymmetric modes that yield a time averaged vanishing total perpendicular divergence of flows, with the parallel divergence representing a small correction [5]. The remaining plot in the same figure diagnoses the radial profile of the nonaxisymmetric part of the fluctuations in the toroidal direction [1]. It shows a typical electromagnetic ITG turbulence signature for the edge region [6], with flat profiles and the fluctuations in ion temperature being the most pronounced quantity. In the SOL, the signature is typical of interchange dynamics, with the electrostatic potential becoming the stronger quantity and the increase in the nonadiabatic electron density ($\tilde{h}_e = \tilde{n}_e - \tilde{\phi}$) due to the decreasing in the coupling between $\tilde{n}_e$ and $\tilde{\phi}$ as the convective cell mode is allowed in the SOL [4]. From the sharp transition between the two regimes, one estimates a shear layer width of about $15\rho_s$, which is in accordance with experimental observations of $\sim 1cm$ [8, and references therein].

The morphology of axisymmetric component of the $\tilde{A}_\parallel$ (magnetic potential) and the parallel current $\tilde{J}_\parallel$ (not shown) yield the side band structure representing the equilibrium Pfirsch-Schlűter currents, the rest state of the global Alfvén wave mode. For the latter, this is only seen in the edge region, with the SOL being dominated by the Debye losses into the limiter plates. The remaining state variables (electrostatic potential, densities and temperatures) are mostly zonal in the edge region, although the side-band structure is still visible. In the SOL, especially
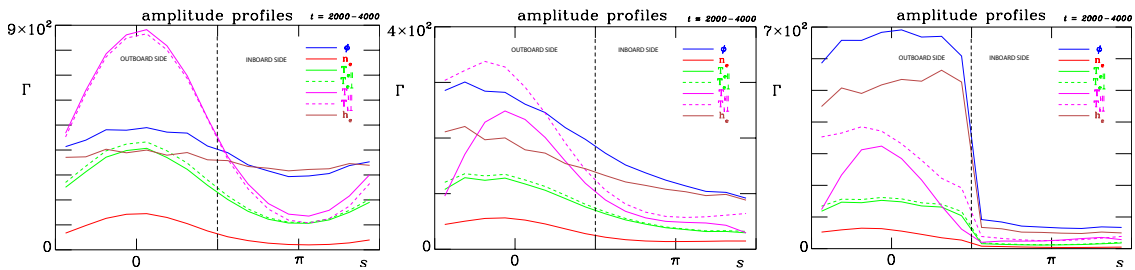

Figure 2: Parallel mode structure: time averaged envelopes of the squared amplitudes $k_y \neq 0$ part of $\tilde{\phi}$ ('p' – blue), $\tilde{n}_e$ ('n' – red) and $\tilde{h}_e$ ('H' – green) vs. the parallel coordinate s.

for $\tilde{\phi}$, $\tilde{n}_e$ and $\tilde{T}_{i\perp}$, there is a clear change in the equilibrium evidenced by the differences between inboard and outboard sides for the DL case, which are isolated from each other. On top of that, and easier to observe in the SL case, there is change in the side-band part of the state variables, compared to the edge region, which can only be a consequence of the change in the mean drifts (diamagnetic and $E \times B$) between edge and the SOL, recalling the shear layer across the last closed flux surface (LCFS).

Fig. 2 shows the parallel mode structure for the (a) edge and (b and c) the SOL region for both SL and DL cases. The ITG signature is again evidenced here for the former, with the interchange character for the $\tilde{T}_i$, which appears strongly ballooned, an an adiabatic response for the electrons [10]. The latter shows the interchange/flute mode signature, with the increase in the role of the $\tilde{\phi}$. Compared to the SL (Fig2b), the DL case (Fig2c), evidences a even stronger dominance of the interchange dynamics as a result of the isolation of the outboard side, from the side where the interchange modes are stable. The differences between those to sides of the plasma are clear in this case, something also seen in the drift plane morphology plot (single snapshot, not time averaged), shown in the last figure, for the DL case. There, structures that extend from the edge to the SOL across the LCFS observed in the outboard side are not present in the inboard side. The very significant differences observed between those regions should allow for comparisons with experimental measurements. This is left for future work, as is the continuation of the study using the inhomogeneous formulation of the theoretical model [11].
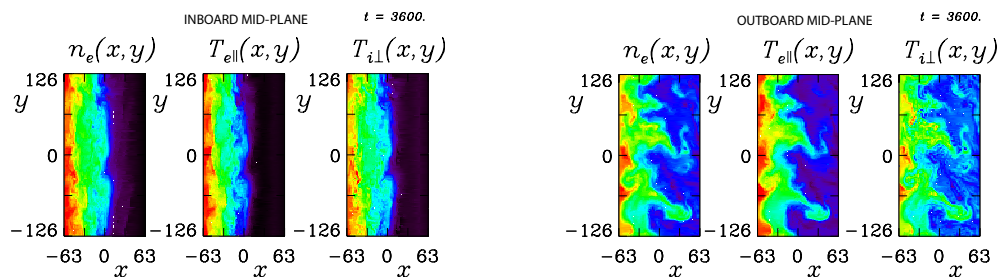
Figure 3: Drift plane morphology at the mid-plane (a) inboard and (b) outboard sides for the DL case.

References
[1] B. Scott 1997 *Plasma Phys. Control. Fusion* **39** 1635
[2] M. Wakatani and A. Hasegawa *Phys. Fluids* **27** (1984) 611
[3] B. Scott *Phys. Plasmas* **5** (1998) 2334
[4] T. T. Ribeiro and B. Scott, *Plasma Phys. Control Phys.* **47** 2005 1657
[5] B. Scott, *Contrib. Plasma Phys.* **46** 2006, accepted
[6] B. Scott *New J. of Phys.* **4** (2002) 52.1
[7] B. Scott *Phys. Plasmas* **12** (2005) 102307
[8] H. Y. W. Tsui *Phys. Fluids B* **4** (1992) 4057
[9] D. R. McCarthy et al. *Phys. Fluids B* **5** (1993) 1188
[10] B. Scott *New J. of Phys.* **7** (2005) 92
[11] D. Strintzi, B. Scott and A. Brizard *Phys. Plasmas* **12** (2005) 052517